nature chemistry

SUPPLEMENTARY INFORMATION

https://doi.org/10.1038/s41557-018-0003-1

In the format provided by the authors and unedited.

Observation of the adsorption and desorption of vibrationally excited molecules on a metal surface

Pranav R. Shirhatti[1,2,8], Igor Rahinov[3], Kai Golibrzuch[1,2,4], Jörn Werdecker[5], Jan Geweke[1,5], Jan Altschäffel[1,2], Sumit Kumar[2], Daniel J. Auerbach[1,2], Christof Bartels[1,6] and Alec M. Wodtke[1,2,7]*

[1]Institute for Physical Chemistry, Georg-August University of Göttingen, Göttingen, Germany. [2]Department of Dynamics at Surfaces, Max Planck Institute for Biophysical Chemistry, Göttingen, Germany. [3]Department of Natural Sciences, The Open University of Israel, Raanana, Israel. [4]Photonic sensor Technology, Laser-Laboratorium Göttingen e.V, Göttingen, Germany. [5]École Polytechnique Fédérale de Lausanne, Lausanne, Switzerland. [6]Physikalisches Institut, Universität Freiburg, Freiburg, Germany. [7]International Center for Advanced Studies of Energy Conversion, Georg-August University of Göttingen, Göttingen, Germany. [8]Present address: Tata Institute of Fundamental Research, Serilingampally Mandal, Ranga Reddy District, Hyderabad, India.
*e-mail: alec.wodtke@mpibpc.mpg.de

Contents:

(1) Presence of TD* component in the $v = 2 – 2$ scattering channel

Time of flight (TOF) measurements for the $v = 2 – 2$ channel at a scattering angle of 60° are shown below (figure 1, 3rd column). Because the trapping probability is low, the TD* component in the $v = 2 – 2$ channel is much weaker than the DS component. By contrast, in the $v = 2 – 1$ channel the TD* channel is relatively easy to observe since the vibrational relaxation probability in the DS channel is also small and similar in magnitude to the small trapping probability.

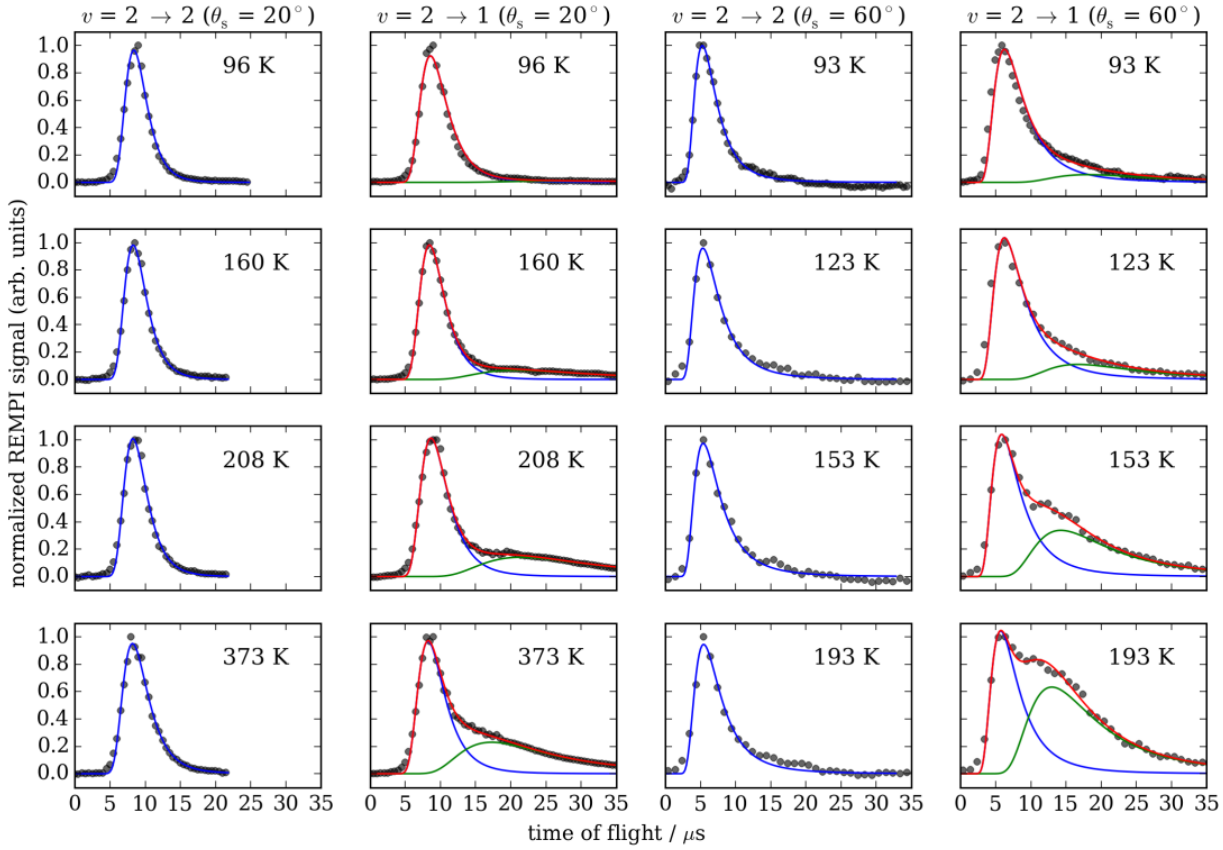

Figure 1: TOF curves at several surface temperatures, including the $v = 2 – 2$ scattering at $\theta_s = 60°$ (see 3rd column). The presence or absence of the TD* component in the $v = 2 – 2$ channel is inconclusive based on these observations alone.

To detect TD* in the 2-2 channel we have performed a different kind of TOF measurement. The scheme for this experiment is shown in figure 2, which we refer to as 2D-TOF[1]. In the 2D-TOF, CO molecules are pumped by an IR laser to $v = 2$, about 1 mm in front of the surface. After scattering from the surface they are pumped by a UV "tag" laser to the metastable $a^3\Pi$ state. The $a^3\Pi$ molecules then travel an additional 18 mm to a point where they are ionized by 1+1 REMPI via the $b^3\Sigma^+$ state. This experiment allows for two delays to be independently controlled: that between the IR laser and the UV tag laser (t_1) and that between the tag laser and the REMPI laser (t_2). By varying t_1, we can perform a low resolution velocity pre-selection, prior to the TOF measurement carried out by varying t_2.

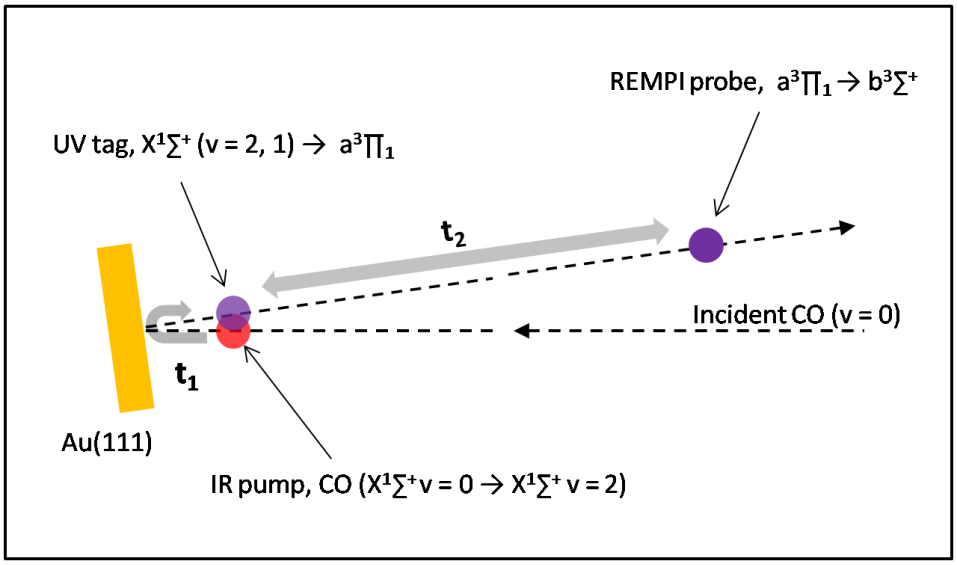

Figure 2: Schematic representation of the 2D-TOF method. Incident CO molecules in the ground state, $X^1\Sigma^+$ $v = 0$ are first pumped to the $X^1\Sigma^+$ $v = 2$ state using an IR laser (IR pump). After waiting for a time delay of t_1 (which allows the faster molecules in the DS component to move further away from the UV tag spot), the scattered molecules in $X^1\Sigma^+$ $v = 2$ and 1 are tagged to the metastable $a^3\Pi_1$ state. These tagged molecules are further probed downstream (using REMPI via $b^3\Sigma^+$) after a time delay of t_2. For appropriate values of t_1 and t_2, this scheme allows us to selectively suppress the large DS component in the $v = 2 – 2$ channel, thereby allowing us to see the relatively small TD* component.

This enables us to selectively suppress the large DS the component in $v = 2 – 2$ channel, making it easier to see the small TD* component. The results of 2D-TOF measurements are shown in figure 3.

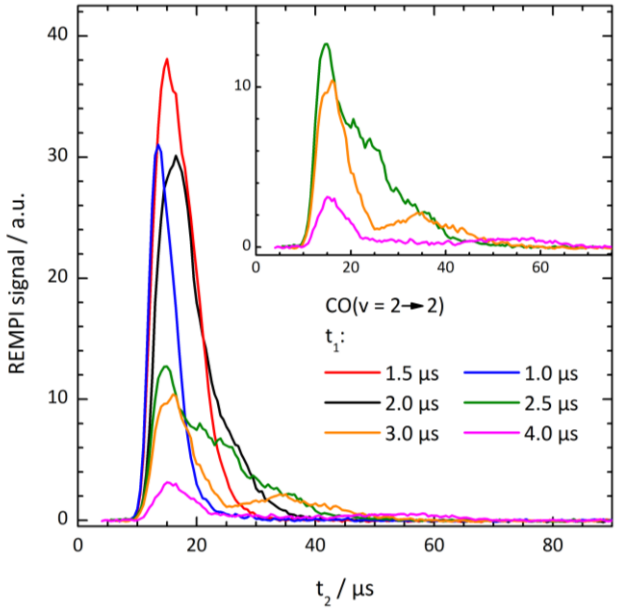

Figure 3: Results of the 2D-TOF measurements for the CO/Au(111) $v = 2 – 2$ channel. As t_1 is increased a second, slow component becomes more visible. We identify this as the TD* component in the $v = 2 – 2$ channel.

At large values of t_1, we pre-select molecules leaving the surface with low speeds. This includes much less of the DS component than in the conventional 1D-TOF measurement. The data of figure 3 clearly show evidence of a fast and a slow component to the overall TOF in the $v = 2 - 2$ channel. We assign the slow channel as the TD* component in the $v = 2 - 2$ channel.

(2) Angular distribution measurements

Figure 4 illustrates how angular distributions were obtained in this work.

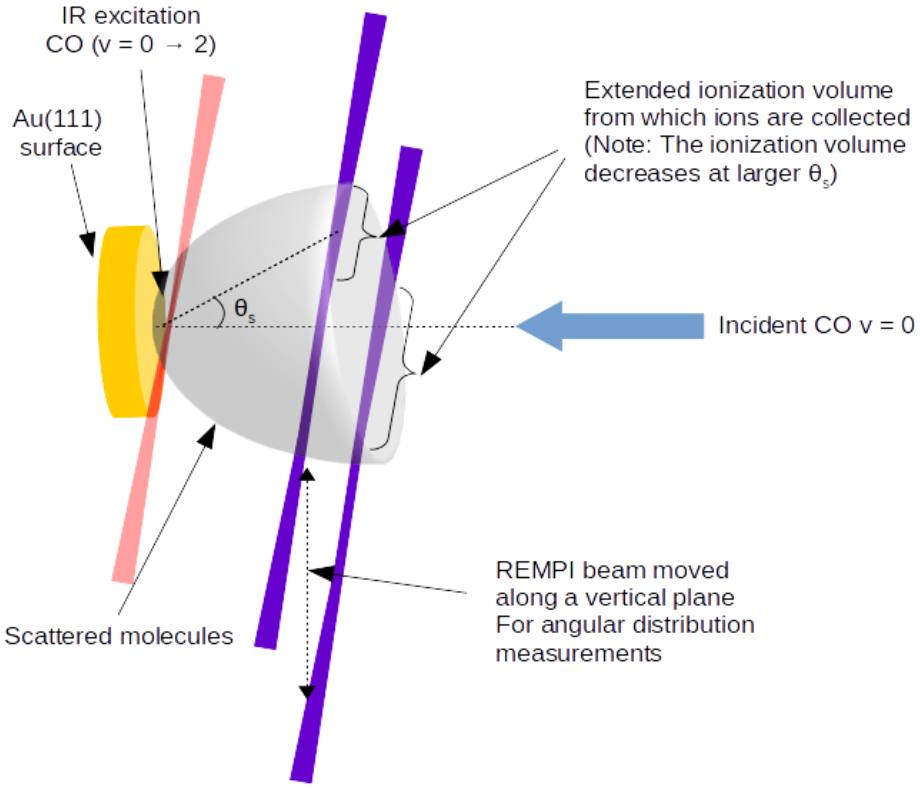

Figure 4: A schematic of the arrangement used for measuring the angular distributions. The probe (REMPI) laser beam runs parallel to the Au(111) surface at a fixed distance of 8.4 mm and is translated parallel to the Au surface in order to vary the detected scattering angle. The REMPI beam was focused 20 mm prior to the vertical plane along which the incident CO molecules are travelling (to minimize non-resonant ionization) and has an extended ionization volume which produces ions along the direction of laser propagation. Due to the cylindrical symmetry of the CO molecule's angular distribution, the contribution to the signal from off-normal CO molecules that are found along the laser's propagation axis drops with increasing angle from the surface normal. Thus, the ion signal measured as a function of the nominal scattering angle at each vertical position drops off more rapidly than if the measurement had been carried out with a point detector

First, TOF distributions were measured at several scattering angles by varying the delay between the IR and UV laser pulses. The scattering angle was varied by moving the laser beam parallel to and at a fixed distance from the Au(111) surface. Note that the sample of vibrationally excited CO molecules is incident at the surface within a rectangular region that is 0.25 mm in the vertical direction (determined by the IR laser focus, indicated by the red beam of Fig 4) and 2 mm in the horizontal

direction (determined by the size of the CO molecular beam). Each TOF distribution was decomposed into DS and TD* components by a fitting procedure whose results are shown in figure 2 of the main text. These contributions were then integrated to get the magnitude of DS and TD* components at each angle. These signals are further corrected for non-uniformities in the ion collection efficiency as a function of angle to obtain the angular distributions shown in figure 2 of the manuscript. The ion collection efficiency correction factor was obtained by measuring the ion signal as a function of REMPI laser position using background CO gas admitted to the chamber by a leak valve.

It is important to understand that the ion signal intensity versus laser beam position measured in this way is more sharply peaked than the true angular distribution (CO flux versus angular deviation from the normal, θ_s). This is due to the fact that the REMPI laser beam is not a point ionizer. The REMPI laser beam ionizes the CO molecules over an extended volume, effectively integrating the signal along the direction of propagation of the laser beam. This is shown in Figure 4. The "laser propagation direction integration volume" decreases as the angle from the surface normal is increased. This causes the signal to drop more rapidly as the laser beam moves away vertically than if the ionization volume were very small. We have modeled this simple geometric effect and find that in the case of trapping desorption without a barrier, where the angular distribution is expected to follow a $\cos\theta$ function, the observed distribution (ion intensity versus vertical position) appears as a $\cos^2\theta$ function. Figure 2 of the main text shows that the measured signals are very close to a $\cos^2\theta$ function, indicating that the TD* channel exhibits a product flux versus θ_s that is close to a $\cos\theta$ function.

(3) Estimating the residence time of CO on Au(111) surface

The residence time (τ_{res}) of an adsorbate at a given surface temperature (T_{s}) can be estimated by the following relation:

$$\tau_{\mathrm{res}} = (k_{\mathrm{des}})^{-1} = [\nu \exp(-E_{\mathrm{des}}/k_{\mathrm{B}}T_{\mathrm{s}})]^{-1} \quad \ldots(1)$$

Here, k_{des} is the desorption rate constant, ν is the desorption frequency factor, E_{des} is the desorption activation energy and k_{B} is the Boltzmann constant. Based on previous temperature programmed desorption (TPD) results for CO on Au(111) under low coverage situations (relevant for our work), the values of ν and E_{des} have been reported to be 2×10^{15} Hz and 0.18 eV, respectively.[2] We point out that this previously published frequency factor (2×10^{15} Hz) is erroneous, possibly due to a typographical error. As a consequence, we have re-analyzed the previously reported TPD results and find $\nu = 3 \times 10^{17}$ Hz. For E_{des}, we obtain 0.18 eV, the same value as reported previously.[2]

The TPD measurements in Ref 2 have been evaluated using the heating rate variation method, where a series of TPD traces are measured at several heating rates. For first order desorption processes (as is the case for CO/Au(111)) the following relation holds true:

$$ln\left(\frac{\tilde{T}_{\mathrm{m}}^2}{\tilde{\beta}}\right) = \frac{E_{\mathrm{des}}}{R\,T_{\mathrm{m}}} + \ln\left(\frac{\tilde{E}_{\mathrm{des}}}{\tilde{R}\,\tilde{\nu}}\right) \quad \ldots(2)$$

The E_{des} and ν can be obtained from the slope and intercept of a linear fit to the plot of $\ln(\tilde{T}_{\mathrm{m}}^2/\tilde{\beta})$ vs. $1/T_{\mathrm{m}}$. Here, T_{m} denotes the temperature (in K) at which the desorption rate is maximum, β denotes the heating rate in K/sec, R is the universal gas constant. The quantities within the logarithm are divided by their own unit to obtain a dimensionless argument and hence are denoted by a tilde on top.

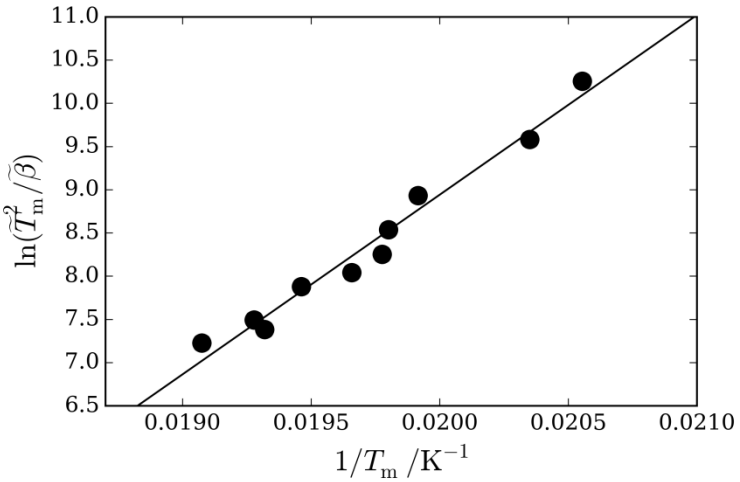

Figure 5: A plot of $\ln(\tilde{T}_{\mathrm{m}}^2/\tilde{\beta})$ vs. $1/T_{\mathrm{m}}$ obtained from TPD measurements reported previously[2] yields a linear trend. The black circles depict the experimentally measured points. The solid line is the best linear fit to the data points.

As seen in figure 5, a plot of $\ln(\tilde{T}_m^2/\tilde{\beta})$ vs. $1/T_m$ (circles) shows a linear trend which is depicted by the line. The parameters for the line of best fit are: (slope) $m = \frac{E_{des}}{R}$ = 2078.12 K, (intercept) $c = \ln\left(\frac{\tilde{E}_{des}}{\tilde{R}\,\tilde{v}}\right)$ = -32.6216 and standard errors: Δm = 116.685 K, Δc = 2.30154.

Using the values of m and Δm we estimate E_{des} = 0.18 ± 0.01 eV. We note that this value is consistent with that reported previously.[2] Using the relation $v = m/e^c$, we obtain v = 3 × 10^{17} Hz. Due to the nonlinear relationship among v and c, Gaussian error propagation is not used for error estimation here. The maximum range for the magnitude of v due to uncertainties in m and c are simply estimated by using $(m - \Delta m)/e^{c+\Delta c}$ and $(m + \Delta m)/e^{c-\Delta c}$ to obtain the lower and upper limits as v(low) = 2.9 × 10^{16} Hz and v(up) = 3.2 × 10^{18} Hz, respectively.

The best estimate values of τ_{res} as a function of T_s, estimated using Eqn. 1 is shown in figure 6 (solid line). The uncertainties in τ_{res} (dashed lines in Fig. 2) were estimated using Eqn. 1 along with the uncertainties in v and E_{des} as follows: $\tau_{res}\,(\text{low}) = [v(\text{up})\exp(-(E_{des} - \Delta E_{des})/k_B T_s)]^{-1}$ and $\tau_{res}\,(\text{up}) = [v(\text{low})\exp(-(E_{des} + \Delta E_{des})/k_B T_s)]^{-1}$

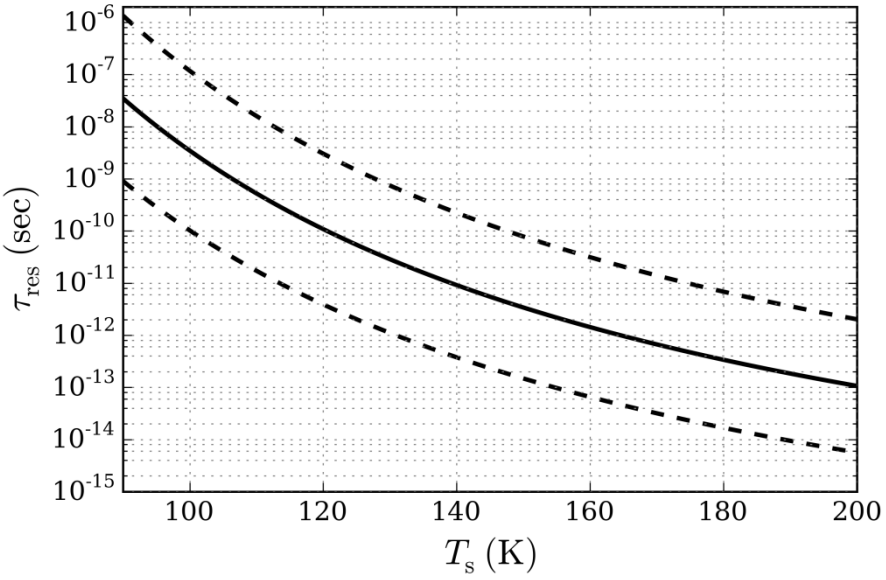

Figure 6: A plot of the estimated residence time of CO on Au(111) at different surface temperatures. The black solid line denotes the best estimate and the dashed lines denote the uncertainties (see text for details).

(4) Model for calculating the translational energy distributions for the TD* component based on detailed balance and normal energy scaling

The model used for obtaining the results presented in figure 4 of the manuscript is described here.

According to the principle of detailed balance the observed translational energy distribution of the TD* component can be expressed as follows:

$$G_{\text{obs}}(E,\theta,T_{\text{s}}) = S(E,\theta) \times F(E,T_{\text{s}}) \qquad (3)$$

Here,

$G_{\text{obs}}(E,\theta,T_{\text{s}})$ = experimentally observed translational energy distribution of the desorbing molecules measured at scattering angle θ and surface temperature = T_{s}.

$S(E,\theta)$ = sticking probability for a given incidence translational energy, E and incidence angle, θ

$F(E,T_{\text{s}})$ = Maxwell-Boltzmann distribution for translational energy at the surface temperature, T_{s} .

In principle, the trapping probability function can be obtained from Eqn. 3 as follows:

$$S(E,\theta) = \frac{G_{\text{obs}}(E,\theta,T_{\text{s}})}{F(E,T_{\text{s}})} \qquad (4)$$

Alternatively, following previous work on trapping desorption[3,4] we assume the trapping probability only depends on normal momentum (normal energy scaling) and use a trapping function of the following form:

$$S(E,\theta) = \frac{1}{(1+\exp[\alpha\, E\, \cos^2\theta + \beta])} \qquad (5)$$

This is essentially a smoothed step function, with α and β as adjustable parameters. In these model calculations, we assume the trapping probability to be described by equation (5), with the following values for the parameters: α = 100 and β = -3.0. The choice of the parameters is made such that there is reasonable agreement with the trapping function obtained from the experimental data by application of equation (4) (see figure 7).

Using this expression for the sticking probability, we are able to calculate the kinetic energy distributions for any given surface temperature and scattering angle. A comparison of the mean values

of the translation energy distributions obtained from the above model with experimental results is shown in figure 4 of the manuscript.

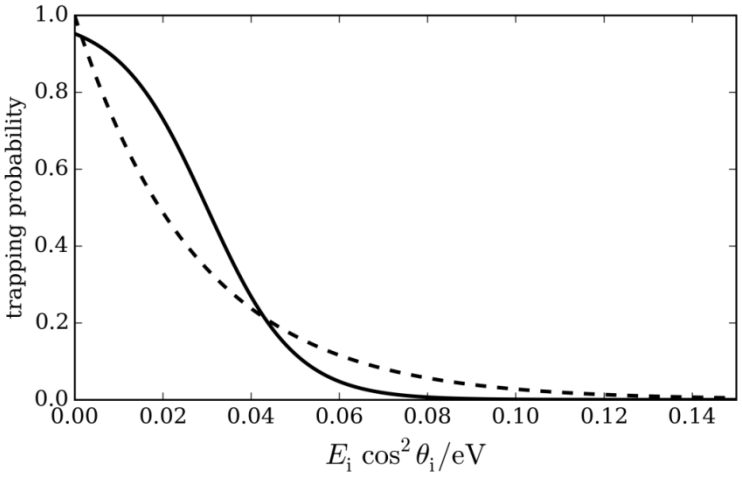

Figure 7: (Solid curve) Trapping probability vs. incidence energy, as described by equation (5), used for calculating the translational energy distributions at a given angle and surface temperature. (Dashed curve) trapping probability vs. incidence energy obtained from the experimentally measured translational energy distributions using equation (4) (T_s, = 300 K, θ_s = 2.8°).

(5) Rotational distributions for the DS and TD* components

The information about the rotational state distributions for the scattered CO (v = 1) was obtained from the analysis of the resonantly enhanced multi-photon ionization (REMPI) spectra. The REMPI spectra for the DS (fast) and TD* (slow) components were selectively measured by setting an appropriate delay between the IR (pump) and the UV (probe: REMPI) laser. Results of such measurements were obtained for four different surface temperatures and are shown in figure 8. The spectra shown here are in the region of the collapsed v = 1 – 1 Q-branch of the $X^1\Sigma^+$- $B^1\Sigma^+$electronic band system. This feature probes all the rotational states of the CO v = 1. The two additional peaks on either side of the Q branch are CO v = 0 – 0, O(8) and O(9) rotational lines. These probe CO v = 0 and are only weakly dependent on surface temperature.

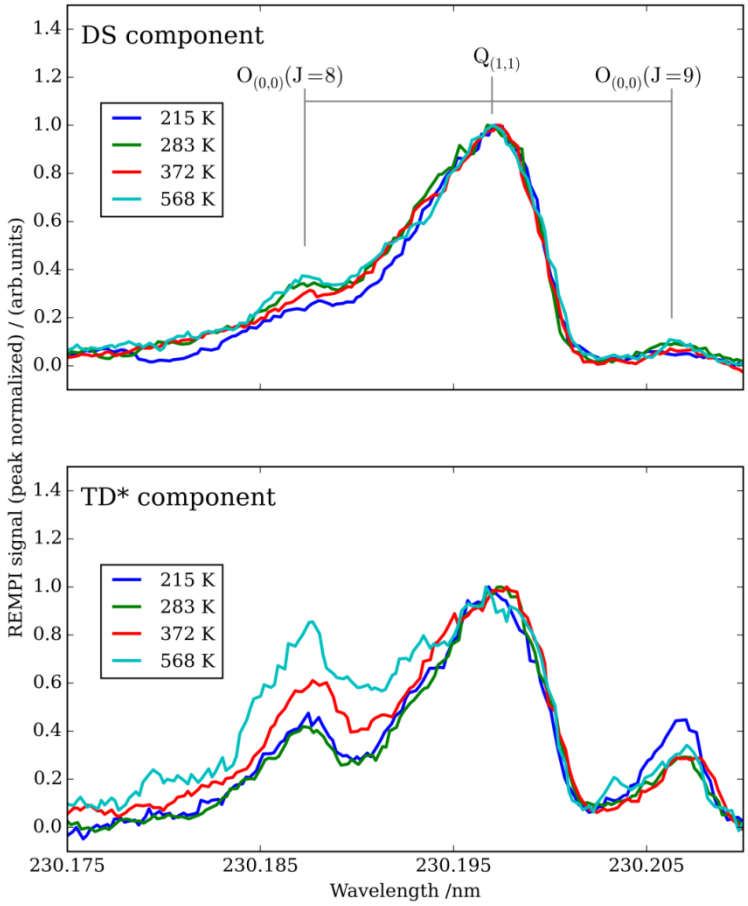

Figure 8: Resonantly enhanced multiphoton ionization (REMPI) spectra (peak normalized) of the scattered CO (v = 2 – 1) molecules measured at several surface temperatures for the DS (upper panel) and TD* (lower panel) components. The REMPI spectra measured for the DS component show little change with increasing T_s, indicating that the rotational distributions are only weakly dependent on T_s (as expected for the DS channel). In contrast, the rotational distributions measured for TD* component clearly exhibit a much larger change with increasing T_s (as expected for the case of trapping-desorption).

These spectra show that the rotational contour of the TD* channel is much more sensitive to surface temperature than is the corresponding spectral feature associated with the DS component. Similar spectra were fitted (figure 9) as a sum of the CO v = 1 Q-branch (blue) and CO v = 0 O-branch (green) contributions, with the rotational temperature of the v = 1 band as a fit parameter. The rotational temperature of the CO (v = 1) molecules produced through the TD* channel increases with surface temperature in the TD* channel. See figure 6 of the main article.

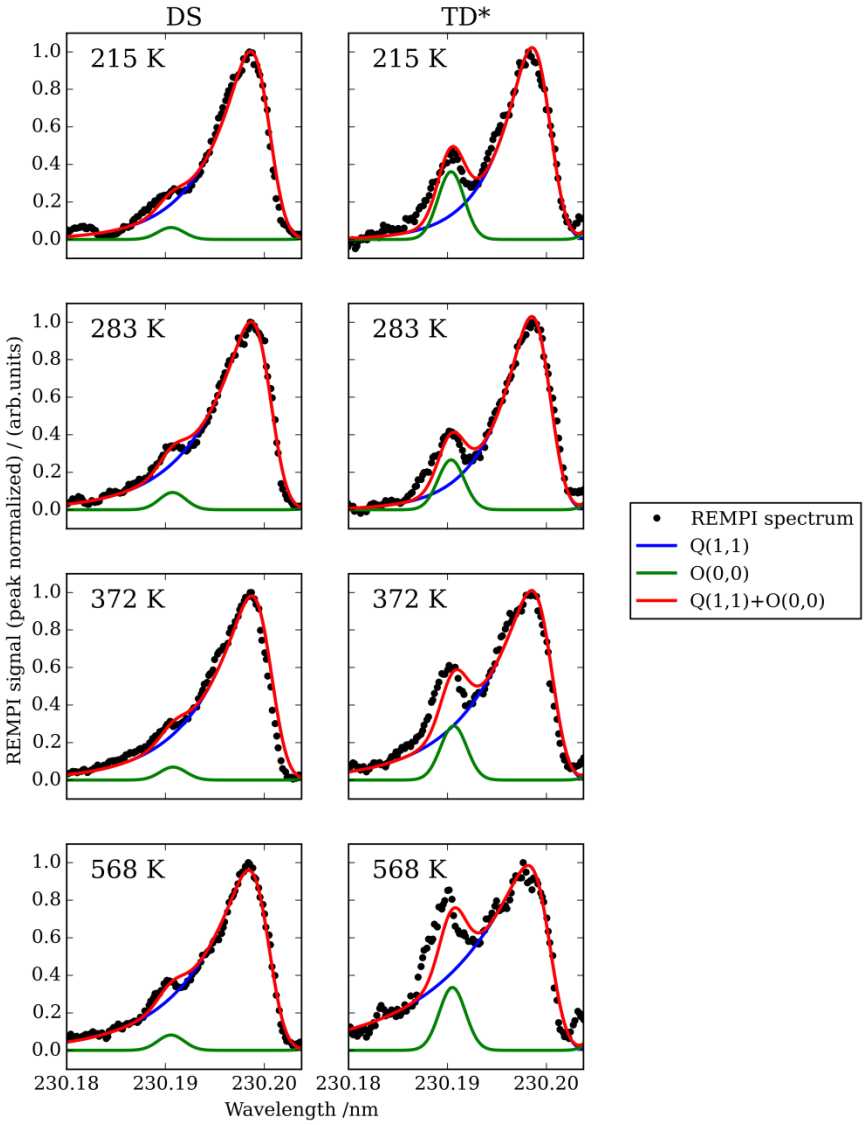

Figure 9: REMPI spectra along with the fit for scattered CO v = 1, measured for the DS (left column) and TD* (right column) component. The spectra were modeled as a sum of Q(1,1) (blue) and O(0,0) (green) branch lines with the rotational temperature of the CO v = 1, Q(1,1) band as a fit parameter. In the case of TD*, the Q(1,1) band is seen to broaden as the surface temperature increases, providing a clear indication of increasing rotational temperature with increase in T_s. In contrast, for the case of DS component this dependence is much weaker.

(6) Infrared spectra of CO adsorbed on Au(111)

Vibrational spectra of CO adsorbed on a clean Au(111) surface were measured using infrared reflection absorption spectroscopy (IRRAS). These measurements were carried out in a separate experimental apparatus, independent of the scattering experiments described in the methods section of the manuscript. A brief description of the experiments is provided below.

A clean Au(111) surface (orientation accuracy better than 0.1°, purity 99.999 %, MaTeck GmbH) under UHV conditions (base pressure 1.7×10^{-10} Torr) was prepared by sputtering (3 keV Ar ions, 25 min) and annealing at 1000 K for 20 min. The sample cleanliness was checked by Auger electron spectroscopy, which showed contamination was ≤ 1% of a monolayer.

A sub-monolayer coverage of CO on Au(111) at a surface temperature of 25 K was prepared by dosing the surface with CO gas, let into the chamber via a leak valve. The IR radiation was produced via optical parametric amplification (OPA) using a BBO crystal followed by difference frequency mixing in a $AgGaS_2$ crystal (the resulting pulses have wavelength ~ 5μm, pulse energy ~ 0.1 μJ). The OPA is pumped by a 1 kHz Kerr-lens mode-locked Ti:Sapphire oscillator/regenerative amplifier (pulse width ~150 fs, λ ~ 800 nm).

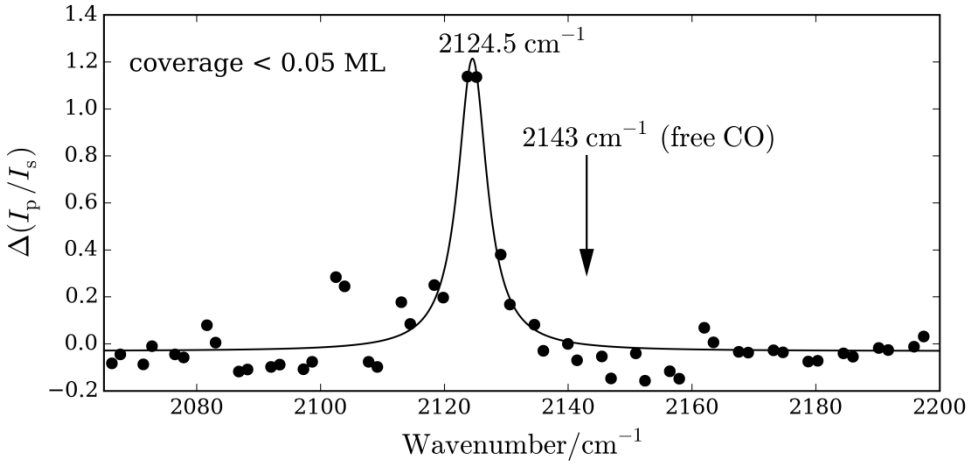

Figure 10: Infrared absorption spectrum of CO adsorbed on a clean Au(111) surface measured under low coverage conditions (coverage < 0.05 monolayers). The points show the results of experimental measurements and the line denotes a best fit to the data points using a Lorentzian function. These measurements were carried out at a surface temperature of 25 K. For the physisorbed CO, the peak of the absorption band appears at 2124.5 cm^{-1}. This corresponds to a red shift of 18.5 cm^{-1} compared to the vibrational energy gap for a free (isolated) CO molecule at 2143 cm^{-1} (denoted by the arrow).

The polarization of the IR beam is rotated by 45º using a λ/2 wave plate and focused on the Au(111) surface using an off-axis parabolic mirror at an incidence angle of 86º. The reflection from the Au(111) surface is split into p and s-polarized components. Both p and s-polarized beams are focused using a lens on the monochromator and their corresponding spectra are imaged on a liquid N_2 cooled

HgCdTe detector array having 2 × 32 pixels. The intensity of the s-polarized beam (I_s) is used as a reference beam to monitor the change in intensity corresponding to p-polarized beam (I_p). The vibrational spectra are obtained by taking difference between (I_p/I_s) in presence and absence of adsorbed CO. One such spectrum obtained at low CO coverage < 0.05 monolayers (ML) is shown in figure 10. The peak corresponding to the CO stretch mode appears at 2124.5 cm^{-1}, which corresponds to a red shift of 18.5 cm^{-1} compared to the vibrational energy gap of 2143 cm^{-1} for isolated CO molecule.[5]

(7) Estimation of vibrational relaxation time using a model based on dipole interacting with free electron gas

For estimating the vibrational relaxation time for CO adsorbed on Au(111) we followed the ideas of Liebsch et al.[6]. This model describes the interaction of an oscillating dipole with the free electrons of the metal, described by a semi-infinite jellium model. Using this model, the vibrational relaxation time (τ_{vib}) of molecules adsorbed on a metal surface can be estimated from the following relation:

$$\tau_{vib} = \left(\frac{3}{2}\,\mu^2\,\frac{\omega}{k_F\,\omega_p}\,\xi(0)\,\frac{C(d-z_0)}{(d-z_0)^4}\right)^{-1} \quad (6)$$

Here,

μ = transition dipole moment

ω = vibrational frequency

ω_p = plasma frequency of the metal

k_F = a wave vector corresponding to the Fermi momentum

$\xi(0)$ = parameter dependent on the electron density (see figure 3 in Ref[6])

d = distance of the point dipole from the surface

z_0 = image plane position

$C(d-z_0)$ = parameter depending on the electron density of the metal (see inset figure 3, Ref [6])

The equilibrium geometry of CO adsorbed on Au(111) is calculated using density functional theory (DFT), from which the parameter d is obtained. These calculations were performed with the FHI-AIMS package[7] with the GGA-RPBE functional including van der Waals corrections[8]. The surface was defined as a 3×3 slab with 4 layers of Au atoms and 20 Angstroms vacuum. In the geometry optimization calculations, upper three layers of the Au surface and the C and O atoms were allowed to

move. The optimization was stopped when the forces on all atoms were smaller than 0.01 eV/Angstrom. This procedure gave a surface to CO center-of-mass distance of 2.702 Angstroms.

For the CO/Au(111) system using the values of μ = 0.1 D (for a weakly interacting physisorbed molecule this is expected to be not very different than the gas phase value [9,10]), ω = 0.25 eV, k_F = 1.21 $\times$ 10^{10} m^{-1} [11], ω_p = 1.37 $\times$ 10^{16} rad/sec [11], d = 2.702 Å (obtained using DFT as described above), z_0 = 0.74 Å (same as that for CO/Cu), $C(d - z_0)$ = 0.5, yields τ_{vib} = 290 ps.

In contrast, a similar estimation for CO/Cu(100) using the parameters reported by Liebsch[6] yields τ_{vib} = 5 ps. The much shorter lifetime calculated here is primarily a result of the much smaller value of d = 1.6 Å used in that calculation. Figure 11 shows the dependence of τ_{vib} on *d*. An error in our DFT calculated value of d would have a significant influence on the estimated value of τ_{vib}. However, we do not expect it to change the qualitative conclusion of this work.

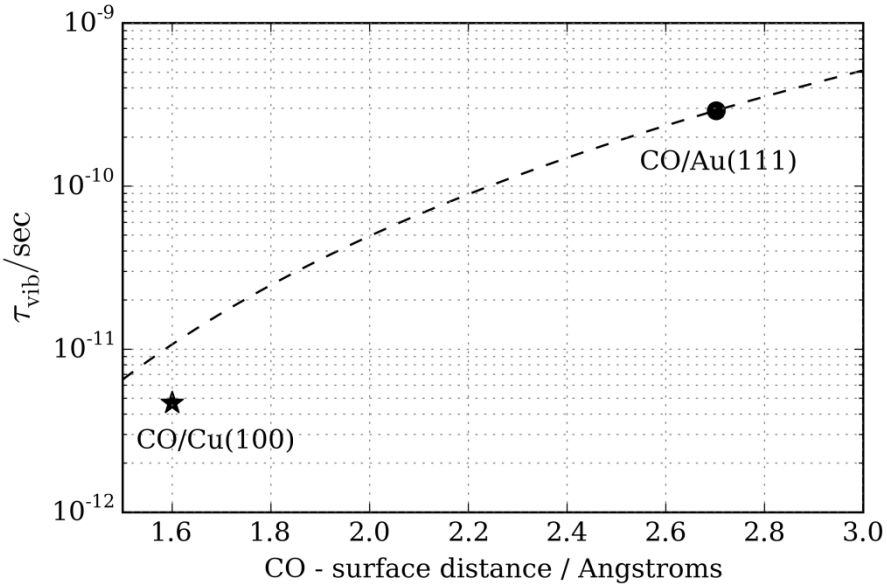

Figure 11: Black circle shows the calculated τ_{vib} for CO/Au(111) using the parameters described above. The dashed line shows the dependence of the τ_{vib} on the parameter *d*. The star symbol shows the results of a similar estimation for CO/Cu(100) system as also reported by Liebsch[6].

References

1. Golibrzuch, K. et al. CO Desorption from a Catalytic Surface: Elucidation of the Role of Steps by Velocity-Selected Residence Time Measurements. *Journal of the American Chemical Society* **137**, 1465-1475 (2015).
2. Engelhart, D.P., Wagner, R.J.V., Meling, A., Wodtke, A.M. & Schafer, T. Temperature programmed desorption of weakly bound adsorbates on Au(111). *Surface Science* **650**, 11-16 (2016).
3. Hurst, J.E., Wharton, L., Janda, K.C. & Auerbach, D.J. Trapping-desorption scattering of Argon from Pt(111). *Journal of Chemical Physics* **83**, 1376-1381 (1985).
4. Rettner, C.T., Schweizer, E.K. & Mullins, C.B. Desorption and trapping of Argon at a 2H-W(100) surface and a test of the applicability of detailed balance to a nonequilibrium system. *The Journal of Chemical Physics* **90**, 3800-3813 (1989).
5. Rank, D.H., St Pierre, A.G. & Wiggins, T.A. Rotational and vibration constants of CO. *Journal of Molecular Spectroscopy* **18**, 418-427 (1965).
6. Liebsch, A. Screening properties of an metal surface at low frequencies and finite wave vectors. *Physical Review Letters* **54**, 67-70 (1985).
7. Blum, V. et al. Ab initio molecular simulations with numeric atom-centered orbitals. *Computer Physics Communications* **180**, 2175-2196 (2009).
8. Tkatchenko, A. & Scheffler, M. Accurate Molecular Van Der Waals Interactions from Ground-State Electron Density and Free-Atom Reference Data. *Physical Review Letters* **102**, 073005 (2009).
9. Chung, C.Y., Ogilvie, J.F. & Lee, Y.P. Detection of vibration-rotational band 5-0 of $^{12}C^{16}O$ X $^{1}\Sigma^{+}$ with cavity ringdown absorption near 0.96 μm. *J Phys Chem A* **109**, 7854-8 (2005).
10. Ogilvie, J.F., L., C.S., Lee, Y.P. & Sauer, S.P.A. Infrared spectra of CO in absorption and evaluation of radial functions fro potential energy and electric dipolar moment. *Theoretical Chemistry Accounts* **108**, 85-97 (2002).
11. Ashcroft, N.W. & Mermin, D.N. *Solid State Physics*, (Harcourt College Publishers, United States of America, 1976).